sustainability

MDPI

Article

Understanding How Physicochemical Properties of Mancozeb and Metalaxyl Shape Onion (*Allium cepa* L.) Production Outcomes: Experimental Stability Studies and Molecular Modeling

Maria M. Savanović [1,2], Đorđe Vojnović [3,4], Andrijana Bilić [1,2], Žarko M. Ilin [3], Igor Savić [5], Teodora Gajo [5], Stevan Armaković [5,*] and Sanja J. Armaković [1,2]

[1] Department of Chemistry, Biochemistry and Environmental Protection, Faculty of Sciences, University of Novi Sad, 21000 Novi Sad, Serbia; maria.savanovic@dh.uns.ac.rs (M.M.S.); andrijana.bilic@dh.uns.ac.rs (A.B.); sanja.armakovic@dh.uns.ac.rs (S.J.A.)
[2] Association of the International Development of Academic and Scientific Collaboration (AIDASCO), 21000 Novi Sad, Serbia
[3] Department of Field and Vegetable Crops, Faculty of Agriculture, University of Novi Sad, 21000 Novi Sad, Serbia; djordje.vojnovic@polj.edu.rs (Đ.V.); zarko.ilin@polj.uns.ac.rs (Ž.M.I.)
[4] Association for Innovation in Sustainable Vegetable Production "INNO4VEG", 22400 Ruma, Serbia
[5] Department of Physics, Faculty of Sciences, University of Novi Sad, 21000 Novi Sad, Serbia; savke@uns.ac.rs (I.S.); dorag@uns.ac.rs (T.G.)
* Correspondence: stevan.armakovic@df.uns.ac.rs

Abstract

This study aims to elucidate the impact of biostimulants and fungicides on onion yield and quality, utilizing a combined experimental and molecular modeling approach. The biostimulants (Humiblack®, Agasi®, and Tifi®) and fungicides (mancozeb and metalaxyl) were applied to onion crops, resulting in significant improvements in onion quality and yield. The stability and environmental impact of mancozeb and metalaxyl alone and in conjunction with biostimulants were investigated. The stability of the fungicide mixture was assessed in ultrapure water and rainwater, revealing high resistance to hydrolysis. Solar stability assessments, conducted using a sun simulator to mimic environmental conditions, highlighted differences in stability between mancozeb and metalaxyl in the presence of biostimulants. Metalaxyl showed higher photostability owing to the benzene ring. It was also less susceptible to biostimulant effects and remained stable in solution. Density functional theory descriptors and frontier orbital analysis rationalized the higher photoreactivity of mancozeb (smaller HOMO–LUMO gap and broader orbital delocalization). At the same time, molecular dynamics simulations supported stronger solvation of mancozeb and short-range water structuring, consistent with enhanced aqueous susceptibility. The results link fungicide physicochemical properties with field performance and aqueous stability, supporting the use of the fungicide mixture together with a single biostimulant as a practical approach for balancing crop productivity and environmental persistence.

Keywords: biostimulants; fungicides; onion quality; stability studies; hydrolysis; direct photolysis; sun simulator; rainwater; density functional theory; molecular dynamics

Check for updates

Academic Editor: Meng Wang

Received: 27 February 2026
Revised: 12 April 2026
Accepted: 22 April 2026
Published: 6 May 2026

Copyright: © 2026 by the authors. Licensee MDPI, Basel, Switzerland. This article is an open access article distributed under the terms and conditions of the Creative Commons Attribution (CC BY) license.

1. Introduction

Onion (*Allium cepa* L.) represents one of the most essential vegetable species and is significant in the daily diet of many people worldwide. Due to its distinctive taste and

aroma, onion is used both fresh as a salad and processed, most commonly dried as a spice or food additive [1,2]. In onion production, the goal is to achieve the highest possible yield and quality, as consumers purchase onions primarily for their quality, especially vitamins, minerals, and various antioxidant compounds [2,3]. It often happens that, due to unfavorable environmental conditions or inadequate application of agronomic practices, both yield and quality fall short of expectations [4]. One approach is the application of various biostimulants, whose mechanisms of action in onion crops have not been sufficiently studied. Consequently, there is a need to examine the effects of biostimulants on onion quality and yield under open field conditions.

Plant growth biostimulants have maintained their position on the market of agricultural input applications [5], which enables the substitution or incorporation of mineral fertilizers. They represent an effective alternative for improving crop quality while minimizing environmental impact [6]. The use of plant biostimulants is expanding as a sustainable approach to enhance crop yields while reducing environmental impact [7–9]. Recent studies have focused on elucidating the influence of biostimulants on the quality and yield of different vegetables [4]. Biostimulant preparations are based on humic substances, free amino acids, marine algae, hydrolysates of proteins, etc. [10]. Within biostimulants, the most promising ones are humic and fulvic acids [11]. They enable sustainable plant growth and terrestrial life in general, and play a role in the regulation of various environmental and ecological processes [12]. Biostimulants containing amino acids and seaweed may increase plant growth and resistance to stress factors. However, it should be noted that each plant variety may exhibit different responses to biostimulant applications [6]. Also, biostimulants based on *Trichoderma strains* are often used to stimulate crop growth and nutrient uptake [13].

Current expectations of the biostimulant use integrate their commercialization alongside crop nutrition. Agronomic activity implementation, combining pesticides and biostimulants, is a crucial approach of agroecological practice because it has significant potential to reduce chemical use, save energy, provide sustainable opportunities for fertilization, and disease management [14].

Modern agricultural production faces the dual challenge of increasing yield while minimizing environmental impact. Pesticides remain an essential component of agricultural production, significantly contributing to yield increase; however, once released into the environment, they represent polluting substances [9,15]. Fungicides are a type of pesticide that prevents the growth of fungi and their spores [16]. The environmental behavior of fungicides has been extensively investigated, and various novel approaches have been proposed to improve the sustainability of agriculture through the reduced use of synthetic agrochemicals such as fungicides [17–19]. An environmentally friendly approach is to use plant biostimulants in combination with fungicides to enhance the quality and yield of crops [20]. Monitoring the stability and behavior of fungicides in mixtures with biostimulants [21] and in the environment is essential to promote sustainable agriculture [22].

Pesticide applications have significantly contributed to agricultural productivity by reducing crop losses. Excessive use of pesticides could lead to occurrences of undesirable residues and contaminants in the environment, and even in living tissues. Pesticides can move from treated agricultural areas into the broader environment. Then they can contaminate surface and groundwater and even react with non-target organisms. Also, pesticides can be transported long distances when they reach the atmosphere [23]. Despite extensive research, predicting pesticide degradation under real environmental conditions remains challenging [24]. Many biotic and abiotic methods are used in the degradation of pesticides, but in some cases, they can lead to toxic degradation products. Therefore, the kinetics of their degradation and mineralization should be carefully monitored. Various

techniques, such as photodegradation, phytodegradation, and biodegradation, could be used to degrade or transform pesticides in the environment [25].

Fungicides represent a vital tool in agriculture, protecting crops from fungal diseases and securing high agricultural yield. The evolution of technology leads to the manufacturing of fungicides, such as chiral fungicides and nanofungicides, with the goal of increasing plant yield and quality. However, the extensive use of fungicides leads to a risk for public health, the environment, and non-target organisms [26]. The long-term environmental fate of fungicides depends on their physicochemical properties. Low degradation rates of fungicides or high adsorption coefficients can determine their accumulation in the groundwater or soil matrix, determining their environmental fate [27].

The aim of this study was to investigate the quality and yield of the onions produced using different biostimulants in combination with fungicides (mancozeb and metalaxyl) under open field conditions. In addition, the stability and environmental behavior of the fungicides were systematically examined. Mancozeb and metalaxyl mixture stability was evaluated in both ultrapure water and rainwater (reflecting the natural way of irrigation). The fungicides were highly resistant to hydrolysis. Furthermore, solar stability was examined, as it represents a key factor in environmental behavior. Environmental conditions were simulated using a sun simulator, and the mancozeb and metalaxyl mixture was examined. Density functional theory (DFT) calculations and molecular dynamics (MD) simulations were used to provide molecular-level insight into the experimentally observed differences in stability, particularly the enhanced photostability of metalaxyl.

2. Materials and Methods

2.1. Chemicals and Solutions

All chemicals were of reagent grade and used without further purification. The commercial formulation of Ridomil Gold® (Syngenta, Hesse, Germany, composition: mancozeb 640 g/kg and metalaxyl-M 40 g/kg, WG water-soluble granules) was used as obtained. The stock solutions of mancozeb (160 mg/dm^3) and metalaxyl mixture (10 mg/dm^3) were prepared using ultrapure and rainwater and stored in a dark place at 25 °C. After rainwater sampling (near Gospođinci), to prevent microbial degradation, rainwater was sterilized by filtration, and glassware was sterilized by autoclaving for 30 min at 140 °C. The biostimulants used and their concentrations were HumiBlack® (DRN Kimya, Antalya, Turkey), based on 15% humic and fulvic acids and 1.7% K_2O (210 mg/dm^3), Tifi® (Italpollina S.P.A., Rivoli, Italy), based on a fungi culture of *Trichoderma atroviride* 2 × 10^8 UFC/g (35 mg/dm^3), and Agasi® (Agafert S.R.L., Bari, Italy), based on SWE (*Ecklonia radiata*, *Laminaria* spp.) with a composition of 2.64% total N, 1.43% total K_2O, and 17.16% organic carbon (60 mg/dm^3). Additional data on applied chemicals can be found in the Supplementary Materials section.

2.2. Field Experiments

A field trial was performed in Gospođinci (45.4059° N, 19.9898° E), located in the Pannonian Basin, one of the most important vegetable-growing regions in Serbia. The size of each experimental plot was 7.5 m^2 (1.5 m width × 5 m length).

Agronomic Practices

In the autumn, a complex NPK 16:16:6 fertilizer (400 kg/ha) was applied, followed by plowing to a depth of 27 cm. In the spring, after pre-sowing preparation, direct seeding of onions was carried out in double rows using Elenka F1 onion seeds (Cora Seeds®, Cesena, Italy). The selected cultivar has bronze-colored dry leaves that have a pleasant aroma, and it is suitable for fresh use as a salad as well as for processing and cooking [28].

Biostimulant treatment included a control (irrigation water and mancozeb and metalaxyl without biostimulants), HumiBlack® (humic and fulvic acid-based) at 50 L/ha, Tifi® (*Trichoderma* spp.-based) at 3 kg/ha, and Agasi® (seaweed extract-based) at 10 L/ha. All biostimulants were used according to the manufacturer's recommended rates. The experiment treatments were arranged in a randomized block setup with three replications and applied in two equal doses via a drip irrigation system. The first dose was applied when the second onion leaf had a diameter of >3 cm, and the second dose when the third leaf had a diameter of >3 cm [29]. The timing of irrigation during the day was assessed using SKU-6440 sensors from Davis Instruments® (Hayward, CA, USA), which were networked with the Vantage ProTM weather station made by the same manufacturer [28]. Pesticides (mancozeb and metalaxyl) were applied using the Ge-WS 18/35 Li E battery-powered sprayer by Einhell® (Landau an der Isar, Germany), which has a battery voltage of 18 V, a tank capacity of 3.5 L, a pressure of 2.5 bar, and a flow rate of up to 60 L/h. The timing of pesticide application was determined based on the recommendations and forecasts from the Agricultural Extension Service Sombor (https://www.psssombor.rs/pis.html (accessed on 1 March 2025)).

2.3. Degradation Procedures in the Sun Simulator

Hydrolysis of the mancozeb and metalaxyl mixture was performed under dark conditions in a volumetric flask (Duran®, Duisburg, Germany). The experiments were conducted at a temperature of 25 ± 1 °C, and hydrolysis was monitored over 30 days in ultrapure and rainwater. Samples were collected in the selected time intervals.

Direct photolysis was carried out using the Sun 2000 simulator, model 11016-1, from ABET Technologies (Milford, CT, USA). The experimental setup data can be found in the Supplementary Materials.

To estimate the exposure of the samples to sunlight, the data from HelioClim-3 for Novi Sad were used [30]. It was determined that 120 min under sun simulator irradiation was equivalent to an annual average of 34 days of natural sunlight. Minimal exposure was calculated to be 15 days for the periods with the most sun hours, while 83 days were calculated for the periods with the least sun hours. The lowest amount of sun hours is obtained in December, while the highest amount of sun hours is obtained in June/July. Details about HelioClim-3 can be found in the Supplementary Materials.

2.4. Analytical Procedures

Ultra-Fast Liquid Chromatography with Photodiode Array Detection (UFLC–PDA, Shimadzu, Duisburg, Germany) was used to monitor the stability of mancozeb and metalaxyl. The details on HPLC procedures, pH monitoring, and procedures applied during the physicochemical characterization of the water samples can be found in the Supplementary Materials.

2.5. Computational Details

Structures of mancozeb and metalaxyl were originally pre-optimized at the GFN2-xTB [31–34] level of theory, using the Atomistica.online 2025 [35–38], an online molecular modeling platform free for academic usage (https://atomistica.online accessed on 15 January 2026). An initial conformational search was carried out using the GOAT [39–41] procedure at the GFN2-xTB level of theory to identify low-energy conformers, as implemented in the ORCA 6.1. [42–47] molecular modeling package. The lowest-energy conformer obtained from this search was subsequently used for higher-level calculations.

Geometry optimizations were then refined at the r2SCAN-3c [48] level of theory, which offers a reliable and efficient balance between computational demand and accuracy for molecular structures.

On the optimized geometries, single-point calculations were carried out using the ωB97X-V [49] functional together with the def2-TZVP [50,51] basis set. The resulting electronic structure data were used to compute global quantum molecular descriptors and to generate frontier molecular orbital (FMO) visualizations. Files necessary for visualization of FMOs with the VMD [52–56] program were obtained using the Multiwfn program [57–60]. The Maestro [61] academic program was also used for molecular visualizations.

MD simulations were conducted to investigate solute–solvent interactions of mancozeb and metalaxyl in an explicit aqueous environment. Each MD system consisted of a single fungicide molecule solvated in approximately 1500 water molecules. The OPLS3e [62–65] force field was employed to describe all molecular interactions, while water molecules were modeled using a simple point charge (SPC) model. MD simulations were conducted with the Desmond program [61,66] within the Schrödinger Materials Science Suite 2022-3 version. MD simulations were conducted at 300 K with a total duration of 20 ns. Nonbonded interactions were treated using a cutoff distance of 9 Å. The resulting trajectories were analyzed to obtain solute–solvent interaction energies and radial distribution functions (RDFs).

2.6. Statistical Analysis

Statistical analysis was performed using one-way ANOVA followed by the LSD test at a significance level of $p < 0.05$, using DataExplorer Online [67] and Statistica Version 14.0.0.15. DataExplorer Online is an online software tool for data analysis available at https://dataexplorer.atomistica.online/ (accessed on 1 April 2026).

3. Results and Discussion

3.1. Onion Quality Assessment

Biostimulants significantly affected the above-ground mass of onion plants (Figure 1). The highest above-ground mass per plant was recorded in treatment T (39.49 g), while the lowest was in treatment A (27.88 g). Compared to the control (C) (33.34 g), treatment T was 18.44% higher, whereas treatment A was 16.37% lower. The advantageous effect of *Trichoderma* spp. on onion biomass yield from direct sowing and onion sets was reported by Vojnović et al. [4].

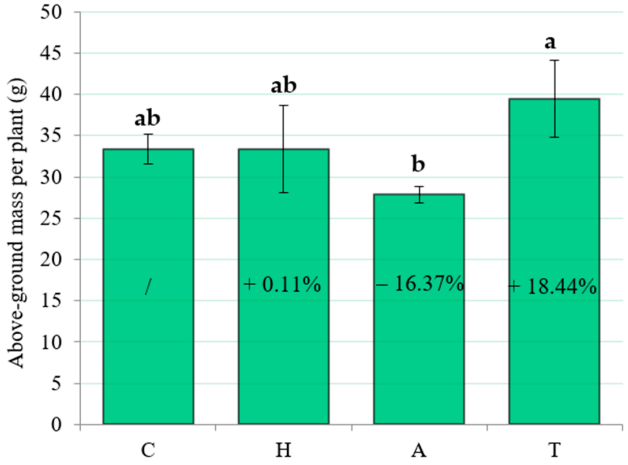


Figure 1. Influence of biostimulants on above-ground mass per plant (g). C—control without biostimulants; H—Humiblack®; A—Agasi®; T—Tifi®. Error bars indicate the standard deviation. Percent values (%) inside the bars indicate the change relative to the C, with positive values showing an increase and negative values a decrease in above-ground mass per plant compared to the C. Means with different letters represent significantly different values at $p < 0.05$ following the LSD test.

The application of different biostimulants affected the bulb mass formation (Figure 2). The highest average bulb mass was recorded in treatment T (181.26 g), while the lowest was in control C (157.62 g), representing an increase of 14.99%. The positive effect of biostimulant T can be attributed to the ability of *Trichoderma* spp. to synthesize hormones and peptides that stimulate root architecture, thereby increasing the uptake of mineral nutrients [68,69].

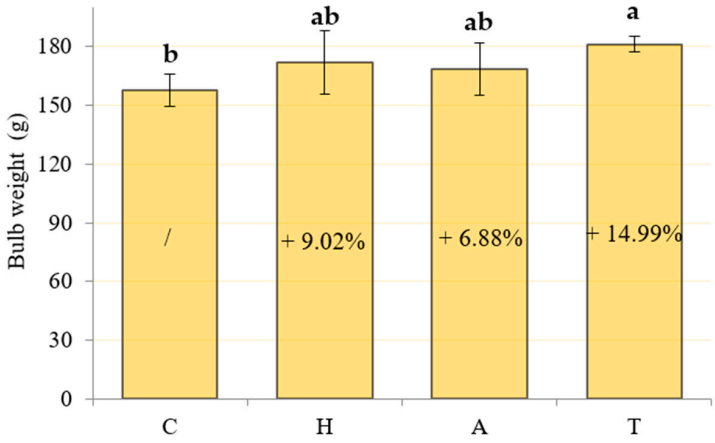


Figure 2. Influence of biostimulants on bulb weight (g). C—control without biostimulants; H—Humiblack®; A—Agasi®; T—Tifi®. Error bars indicate the standard deviation. Percent values (%) inside the bars indicate the change relative to the C, with positive values showing an increase in bulb weight compared to the C. Means with different letters represent significantly different values at $p < 0.05$ following the LSD test.

The dry onion yield was influenced by biostimulant application (Figure 3). The highest dry onion yield was observed in treatment T (8.20 t), which was 26.34% higher than the control C (6.49 t). An increase in onion yield after the application of *Trichoderma* spp. was noted in Vojnović et al. [29]. Treatment H also increased dry matter yield, consistent with findings reported in onion by Hafez et al. [70]. The effect of humic acids may be attributed to their ability to stimulate proton pumps in the tonoplast and plasma membrane [71].

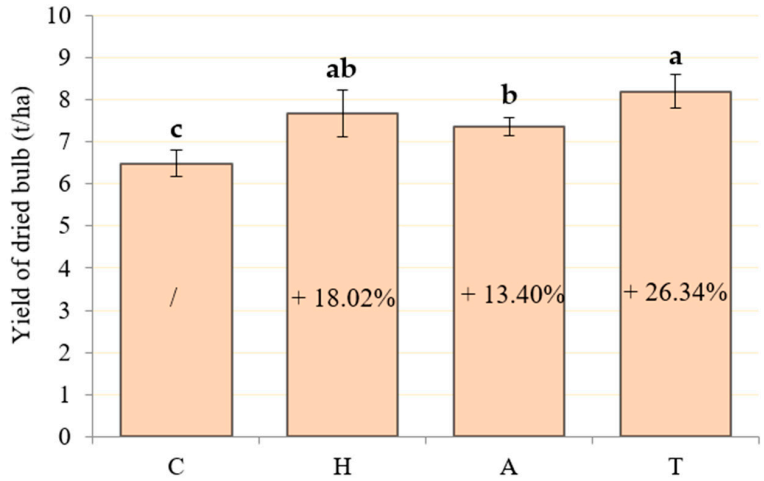


Figure 3. Influence of biostimulants on the dried bulb yield (t/ha). C—control without biostimulants; H—Humiblack®; A—Agasi®; T—Tifi®. Error bars indicate the standard deviation. Percent values (%) inside the bars indicate the change relative to the C, with positive values showing an increase in dried bulb yield compared to the C. Means with different letters represent significantly different values at $p < 0.05$ following the LSD test.

3.2. Changes in Hydrolysis Rate

Hydrolysis was monitored for the mancozeb and metalaxyl mixture since they are used in the field in this form. The process was investigated in ultrapure water and rainwater. Hydrolysis was more pronounced in ultrapure water with 29% of mancozeb and 21% of metalaxyl hydrolyzed (Figure 4). Mancozeb's higher hydrolysis rate is consistent with previous studies, which have shown that mancozeb is unstable in aqueous solution and is susceptible to hydrolysis, forming products such as ethylenethiourea [72]. Metalaxyl's higher hydrolytic stability was consistent with literature data, suggesting that the differences observed in degradation behavior in the mixture are primarily driven by the intrinsic chemical properties of the individual compounds [73]. The hydrolysis rate was reduced in rainwater (19% of mancozeb and 17% of metalaxyl). This suggests that the fraction of fungicides not absorbed by plants may persist longer in the environment under natural irrigation conditions. In rainwater, chloride, sodium, and potassium ions were detected in higher concentrations (Table S1). Chloride, sodium, and potassium may contribute to the inhibition of the hydrolysis of the mancozeb and metalaxyl mixture. The inhibitory effect of chloride and sodium ions on the hydrolysis and photolysis of pesticides has been reported. These ions significantly inhibited the hydrolysis of chlorpyrifos, which has been attributed to reduced interaction between pesticide molecules and water in the presence of ions [74]. It has been reported that chloride ions inhibited the degradation of antibiotics (penicillin G, roxithromycin, oxytetracycline, doxycycline, and sulfamethazine). Antibiotic degradation was reduced from 57% up to 97% depending on the antibiotic [75]. The presence of sodium or potassium reduced the hydrolysis rate of dipeptides. Dipeptides were hydrolyzed between 12 and 18% slower than in the absence of sodium or potassium ions [76].

To capture how the aqueous environment affects the stability and reactivity of mancozeb and metalaxyl, force-field MD simulations were performed.

The MD systems were formed by placing a single fungicide molecule (mancozeb or metalaxyl) in an explicit aqueous environment consisting of approximately 1500 water molecules, ensuring sufficient solvation and minimizing finite-size effects. This setup allows the fungicide to interact freely with the surrounding solvent, closely mimicking dilute aqueous conditions relevant to environmental and experimental photolysis studies. Representative snapshots of the equilibrated MD systems (Figure 5) illustrate the spatial arrangement of water molecules around the mancozeb and metalaxyl molecules.

We first analyze the interaction energies within the fungicide molecules (mancozeb or metalaxyl) and the surrounding water molecules (Table 1). In MD simulations, these interaction energies provide a measure of solute–solvent affinity. They are derived from the nonbonded electrostatic and van der Waals forces between the solute and solvent atoms, as described by the employed force field. The reported values represent time-averaged indicators of solvation strength under the simulated aqueous conditions.

Table 1. Interaction energies between mancozeb/metalaxyl and water.

System	Interaction Energy [kcal/mol]	Hydrolysis Rate (%)
Mancozeb + water	−56.43	29.1
Metalaxyl + water	−53.17	20.8

The total interaction energy between mancozeb and water (−56.427 kcal/mol) is slightly more negative than that obtained for metalaxyl (−53.173 kcal/mol). The results suggest that mancozeb has somewhat stronger interactions with water, compared to metalaxyl. Although the absolute values appear similar, it should be noted that the two fungicide molecules differ substantially in molecular size, with mancozeb consisting of 18 atoms

and metalaxyl of 41 atoms. As a result, the interaction energy is distributed over a larger number of atomic interaction sites in the case of metalaxyl. These results suggest slightly stronger solute–solvent interactions for mancozeb. These interactions may contribute to the higher hydrolysis rate observed for mancozeb compared to metalaxyl.

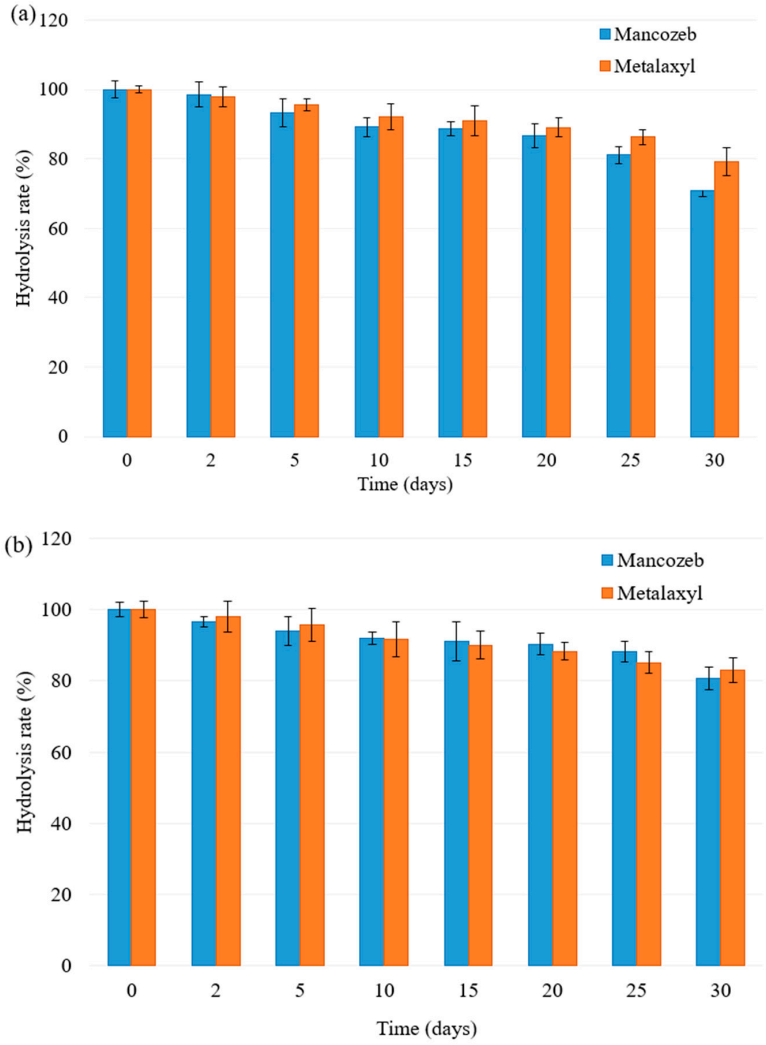


Figure 4. Hydrolysis rate of mancozeb and metalaxyl in (**a**) ultrapure water and (**b**) rainwater.

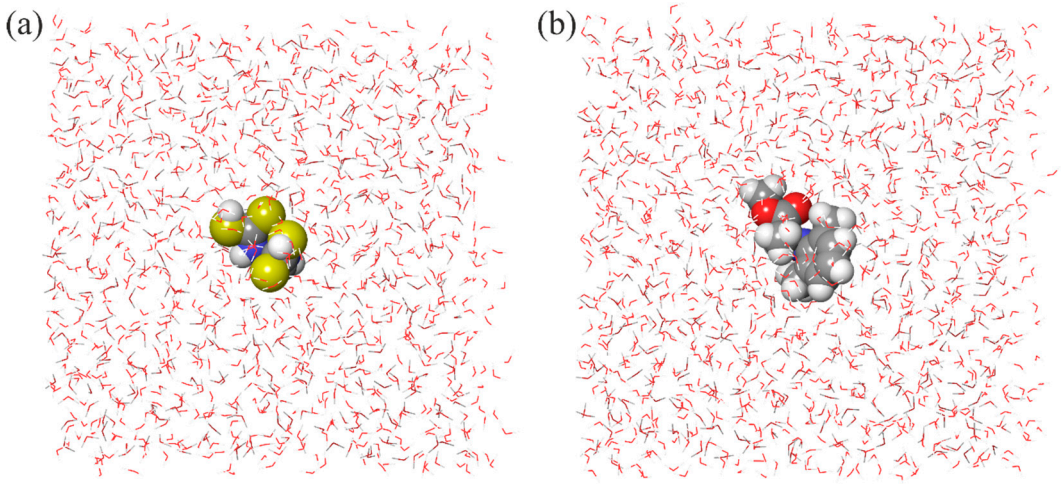


Figure 5. Molecular dynamics snapshots of systems (**a**) mancozeb + water and (**b**) metalaxyl + water.

To quantitatively characterize solute–solvent (mancozeb/metalaxyl − water) interactions and local solvation structure, RDFs were calculated from the MD trajectories. The RDF, g(r), describes the possibility of finding a solvent atom at a proximity r from a selected atom or functional group of the solute, relative to an ideal homogeneous distribution at the same density. RDFs provide detailed information on preferred interaction distances, coordination numbers, and the strength and organization of solvation shells. Peaks in g(r) correspond to structured solvent layers, often reflecting hydrogen bonding or specific electrostatic interactions, whereas flatter distributions indicate weaker or nonspecific solvation. RDFs were calculated for each atom of the fungicide molecules relative to the oxygen atoms of surrounding molecules of water, thereby quantifying the spatial distribution of water around distinct atomic sites of the solute. The RDF results for key atomic sites of mancozeb and metalaxyl are shown in Figure 6.

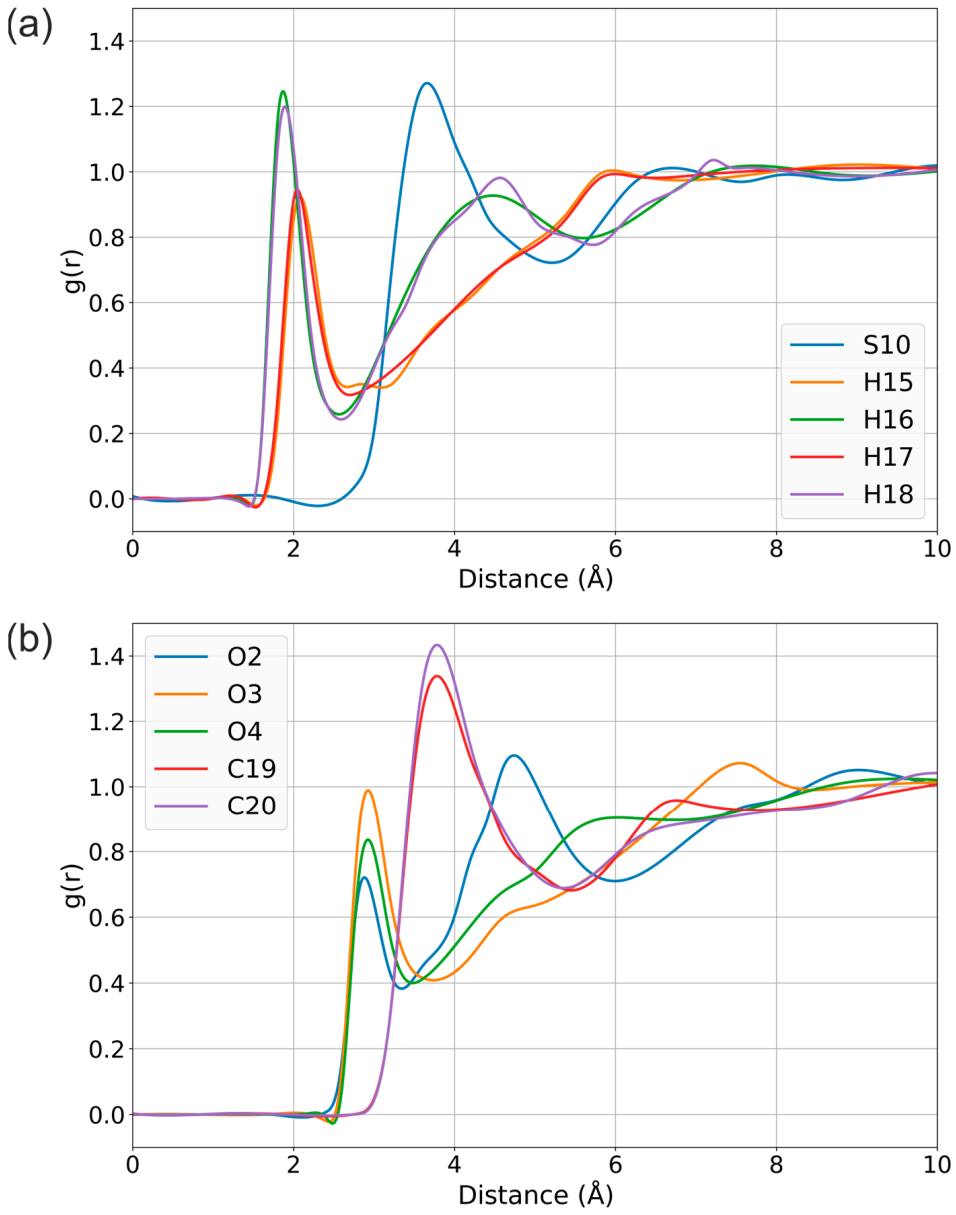


Figure 6. Representative radial distribution functions for molecular dynamics systems (**a**) mancozeb − water and (**b**) metalaxyl − water.

Results in Figure 6 show that the interaction between mancozeb and water is slightly stronger compared to metalaxyl − water interactions. In the case of the mancozeb plus water system, four RDFs involving hydrogen atoms of mancozeb are involved in the very strong interactions with water molecules, characterized by sharp peaks, high g(r) values, and distances of less than 2 Å. These results indicate the formation of strong hydrogen bonding interactions, which may facilitate interactions with water and contribute to enhanced hydrolysis, as indicated by experimental results. While certain RDFs in the case of the metalaxyl plus water system are characterized by sharp peaks and high g(r) values, they are all located at higher distances, of 3 and 4 Å, suggesting weaker interactions between metalaxyl and water.

3.3. Sun Simulator-Induced Photolysis in the Presence of Biostimulants

The stability of mancozeb and metalaxyl mixture was evaluated under sun simulator irradiation in a rainwater matrix and compared with results obtained in ultrapure water. As can be seen from Figure 7, the photolysis of mancozeb was more pronounced than that of metalaxyl. In ultrapure water, the photolysis efficiency of mancozeb was 60%, while metalaxyl photolyzed to an extent of 18%. The high photolysis of mancozeb is consistent with literature data, which have shown that mancozeb is highly susceptible to photolysis in aqueous environments [72]. The lower photolysis of metalaxyl suggests that metalaxyl is relatively photostable under solar irradiation [77]. The addition of biostimulants to the mancozeb and metalaxyl mixture had different effects, depending on the fungicide structure. In the case of mancozeb, photolysis was inhibited with the addition of all three biostimulants (Figure 7a), and it was in the range of 29% to 34%. In addition, the presence of biostimulants affected its stability, which may contribute to prolonged fungicidal activity under field conditions [78] in onion crops in the presence of biostimulants. The addition of biostimulants did not affect metalaxyl stability (Figure 7b), suggesting that its molecular structure is less prone to interaction with the applied biostimulants (Figure S5).

During direct photolysis of the mixture, the initial pH was 5.8 (Figure S6a). After 120 min of photolysis, it increased to 6.6, indicating the formation of alkaline intermediates. The addition of biostimulants increased the initial pH value up to 8.0, while the final pH of the solution was around 7.0. The initial temperature was 25 °C, and it increased to 35 °C during the process (Figure S6b).

Rainwater was collected in areas where onions were cultivated. Investigation of the stability of the fungicide mixtures in rainwater was crucial. The composition of rainwater, including different inorganic ions and organic compounds, can enhance or inhibit the efficiency of degradation of various compounds [79,80]. Following field application, fungicides may be partially washed off from plant surfaces by rainfall and subsequently transported into soil and surface water systems. Assessing their stability and transformation behavior in rainwater is environmentally relevant. To address the influence of rainwater ions, they have been determined within the physicochemical parameters of rainwater and are listed in Table S1. In the next step, the degradation of mancozeb and metalaxyl was performed under the same conditions in rainwater, which represented a natural way of irrigating onion crops. When comparing the degradation of mancozeb in ultrapure water and rainwater, it can be seen that the photolysis of mancozeb was reduced in rainwater. This is relevant for onion production because mancozeb sprayed on the leaf surface is being washed by rainfall and simultaneously interacts with ions present in rainwater. Mancozeb stability in environmental conditions influences maintaining its activity against fungi during onion growth. Namely, the efficiency of mancozeb direct photolysis decreased from 60% in ultrapure water (Figure 7a) to 11% (Figure 8a) in rainwater. In this case, ions detected in rainwater significantly influenced mancozeb photolysis. Its photolysis may have been inhibited by

chloride, sodium, and potassium ions [81]. The addition of biostimulants did not affect the stability of mancozeb. Only in the case of Humiblack®, its stability slightly increased (Figure 8a, photolysis rate 7%). Structural analysis (Figure S5) suggests that the presence of a stable aromatic ring in metalaxyl contributes to its higher stability [73], which is not the case with mancozeb, explaining metalaxyl's higher stability. In rainwater, metalaxyl stayed stable, and its photolysis rate in the presence/absence of biostimulants was very similar to that in ultrapure water (Figures 7b and 8b).

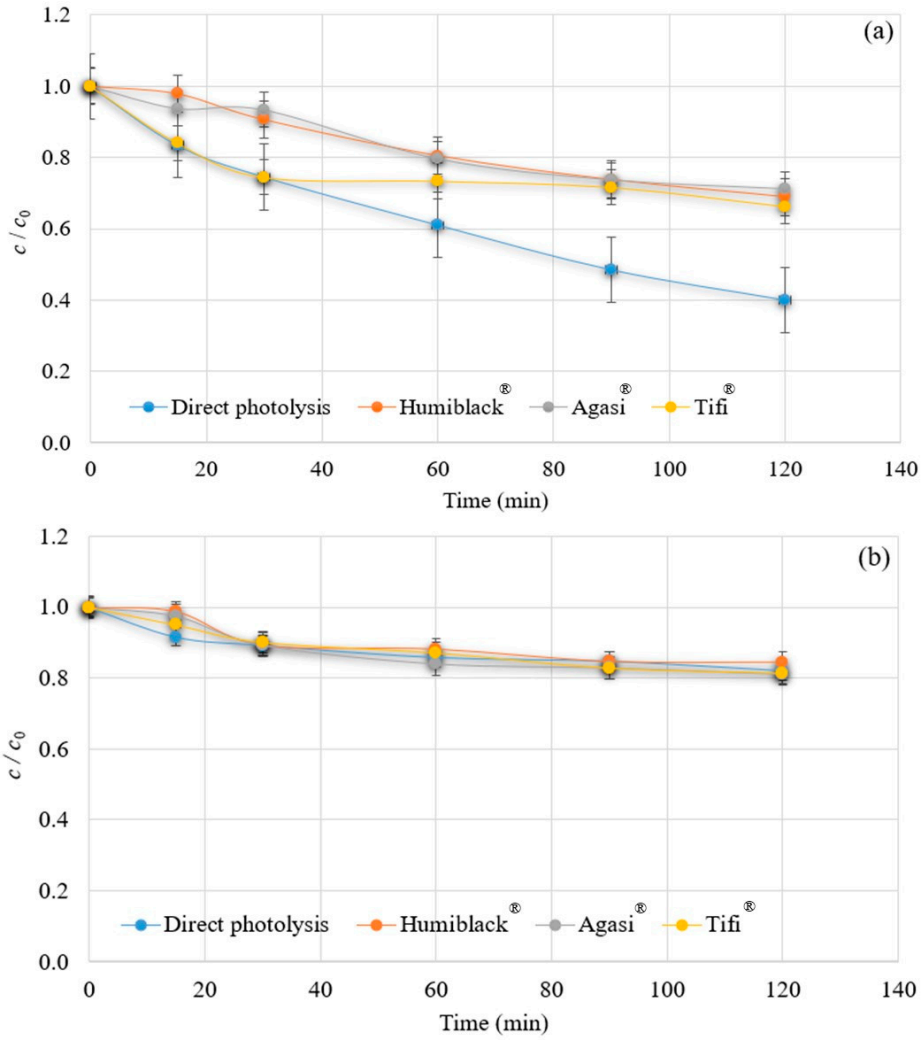


Figure 7. Influence of Humiblack®, Agasi®, and Tifi® on the direct photolysis of (**a**) mancozeb and (**b**) metalaxyl in ultrapure water.

The pH values of the treated solutions in rainwater were around 9.0, and during degradation, they decreased up to 7.0 (Figure S7a), pointing out the formation of acid intermediates. The initial temperature in the sun simulator was 25 °C, while during degradation, it increased to 35 °C (Figure S7b).

The results that were obtained lead to the conclusion that it is optimal to use mancozeb and metalaxyl fungicides in combination with one biostimulant. Humiblack® slightly stands out in the case of metalaxyl, but all three contributed to the efficient time maintenance of mancozeb and metalaxyl to act on onions and provide high-quality crop yield.

The experimentally observed direct photolysis behavior of mancozeb and metalaxyl in ultrapure water (Figure 7) shows a pronounced difference in degradation kinetics. In the absence of biostimulants, mancozeb undergoes faster photodegradation compared to metalaxyl, whereas metalaxyl exhibits high resistance toward direct photolysis under

simulated solar irradiation. To understand the experimental results at the molecular level, DFT calculations were conducted in order to investigate the electronic structure and reactivity descriptors of both fungicides. First, quantum molecular descriptors were calculated based on the frontier molecular orbitals, and these values are given in Table 2.

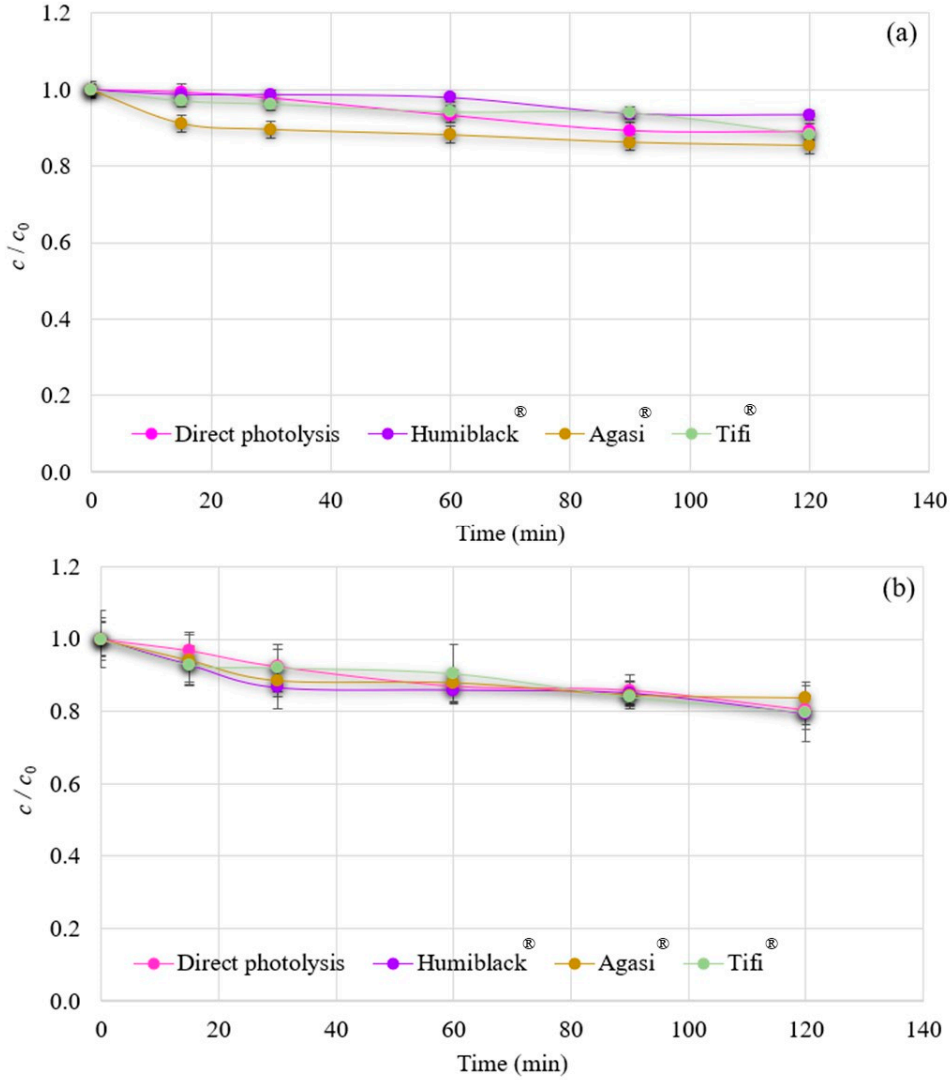


Figure 8. Influence of Humiblack®, Agasi®, and Tifi® on the direct photolysis of (**a**) mancozeb and (**b**) metalaxyl in rainwater.

Table 2. Global quantum molecular descriptors of mancozeb and metalaxyl.

Quantity	Value	
	Mancozeb	**Metalaxyl**
E_{HOMO} [eV]	−8.79	−9.15
E_{LUMO} [eV]	0.86	1.58
Δ*E* gap [eV]	**9.66**	**10.74**
η [eV]	4.83	5.37
S [eV^{-1}]	0.21	0.19
μ [eV]	−3.97	−3.78
χ [eV]	3.97	3.78
ω [eV]	**1.63**	**1.33**

The frontier molecular orbital energies and derived global reactivity descriptors are calculated and given in Table 2. Mancozeb exhibits a smaller HOMO–LUMO energy gap (ΔE = 9.66 eV) compared to metalaxyl (ΔE = 10.74 eV). Since the HOMO–LUMO gap represents the minimum electronic excitation energy, a lower gap suggests that mancozeb can be more readily excited upon absorption of incident solar radiation. This enhanced excitation ability provides a molecular-level explanation for the higher efficiency of mancozeb direct photolysis observed experimentally. Metalaxyl shows a substantially larger HOMO-LUMO gap, indicating a lower probability of photoinduced electronic transitions under the same irradiation conditions, which is consistent with the experimentally observed slower photodegradation in ultrapure water. The smaller HOMO–LUMO energy gap of mancozeb indicates a higher susceptibility to photoinduced electronic excitation, which is in alignment with experimentally observed higher reactivity compared to metalaxyl, under the same conditions.

While chemical softness and potential did not show a significant difference, it was found that the electrophilicity index (ω) differs between the two fungicides, with mancozeb showing a higher value (ω = 1.63 eV) compared to metalaxyl (ω = 1.33 eV). A higher electrophilicity index indicates a greater tendency to participate in charge-transfer processes following excitation, which can lead to bond weakening and subsequent degradation pathways during photolysis. Electrophilicity is associated with the ability of a chemical species to accept a pair of electrons to bond with a nucleophile, therefore facilitating relevant environmental transformations.

Beyond explaining the different photolysis efficiencies observed in water, the calculated global reactivity descriptors also suggest that mancozeb is intrinsically more reactive than metalaxyl in a broader chemical sense. Such global reactivity characteristics imply that, in complex chemical environments, mancozeb can interact more strongly with other electron-rich or electron-deficient molecules. Therefore, global reactivity descriptors can be used to predict molecules' environmental stability and to imply possible reactions.

This enhanced reactivity provides a molecular-level explanation for the experimentally observed influence of biostimulants on fungicide stability. Biostimulant formulations typically contain complex mixtures of organic constituents (e.g., humic substances, amino acids, polysaccharides) bearing multiple polar and electron-donating functional groups. Although explicit modeling of fungicide–biostimulant interactions was beyond the scope of the manuscript, such functional diversity may enable noncovalent interactions (e.g., hydrogen bonding or polar associations) with reactive fungicide molecules. Considering its higher electrophilicity and smaller HOMO–LUMO gap, mancozeb may be more susceptible to electronic perturbation in such heterogeneous environments, which could contribute to the experimentally observed modulation of its photolysis behavior. The electronically more stable and less reactive metalaxyl molecule is less affected by these interactions, consistent with its comparatively weak response to biostimulant presence observed experimentally.

While global electronic descriptors such as the HOMO–LUMO energy gap, hardness, and softness provide quantitative insight into the photochemical reactivity of a molecule, they do not directly reveal where within the molecular framework photoinduced electronic processes are most likely to occur. To obtain spatially resolved information on potential charge-transfer pathways, visualization and analysis of the frontier molecular orbitals are essential.

In the context of photolysis, knowing the molecular sites where frontier molecular orbitals are located is of great importance, as this allows identification of reactive sites and functional groups that govern the molecule's response to solar irradiation. By correlating orbital distributions with experimentally observed degradation behavior, a mechanistic

understanding of structure–reactivity relationships can be established beyond purely energetic considerations. For these reasons, we have visualized HOMO and LUMO orbitals and presented them in Figure 9.

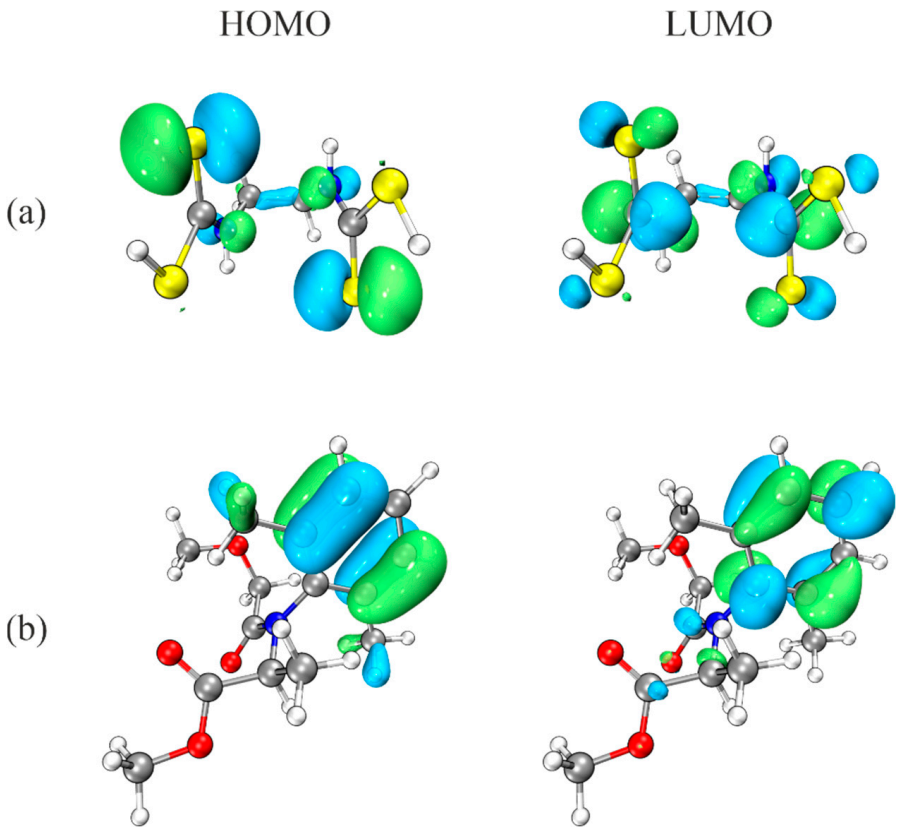


Figure 9. Visualization of the frontier molecular orbitals (HOMO and LUMO) (**a**) mancozeb and (**b**) metalaxyl.

Visualization of the frontier molecular orbitals (FMOs) presented in Figure 9 further supports the experimentally observed higher efficiency of direct photolysis of mancozeb in ultrapure water compared to metalaxyl. In the case of mancozeb, both the HOMO and LUMO are broadly delocalized over nearly the entire molecular framework. This indicates that photoinduced charge redistribution is not confined to a single functional moiety but involves a substantial portion of the molecule.

Such extensive orbital delocalization suggests that upon light absorption, electronic excitation can induce charge transfer across multiple bonds and functional groups, thereby increasing the likelihood of bond weakening and subsequent degradation pathways. Only minor regions of the molecule, primarily associated with specific sulfur-containing groups, show negligible contribution from the HOMO, whereas the LUMO density extends to these sites as well, indicating their potential involvement in excited-state processes.

The FMOs of metalaxyl are strongly localized, with both the HOMO and LUMO predominantly centered on the benzene ring. This pronounced localization implies that photoinduced electronic transitions and charge redistribution are largely restricted to a single aromatic moiety, leaving the remainder of the molecular structure comparatively unaffected by direct light absorption. As a result, only a limited fraction of the molecule participates in photochemical processes, which contributes to the photostability of metalaxyl observed experimentally.

The next step in this study was to examine the behavior of fungicides when combined with a biostimulant mixture and to estimate whether it is economically worthwhile to use more biostimulants on the same onion crops during one season. First, their action was examined in ultrapure water. As aforementioned, direct photolysis of mancozeb was high in ultrapure water (60%). The addition of biostimulant combinations such as Humiblack® + Agasi® and Humiblack® + Agasi® + Tifi® leads to a higher degradation of mancozeb (71% and 83%, respectively, Figure 10a), marking these processes as unfavorable. Metalaxyl photolysis was low because of its higher stability. The high stability of this molecule was reflected in its behavior in a biostimulant mixture, wherein metalaxyl remained stable. Only the use of the mixture of Humiblack® + Tifi® increased its photolysis to 32% (Figure 10b).

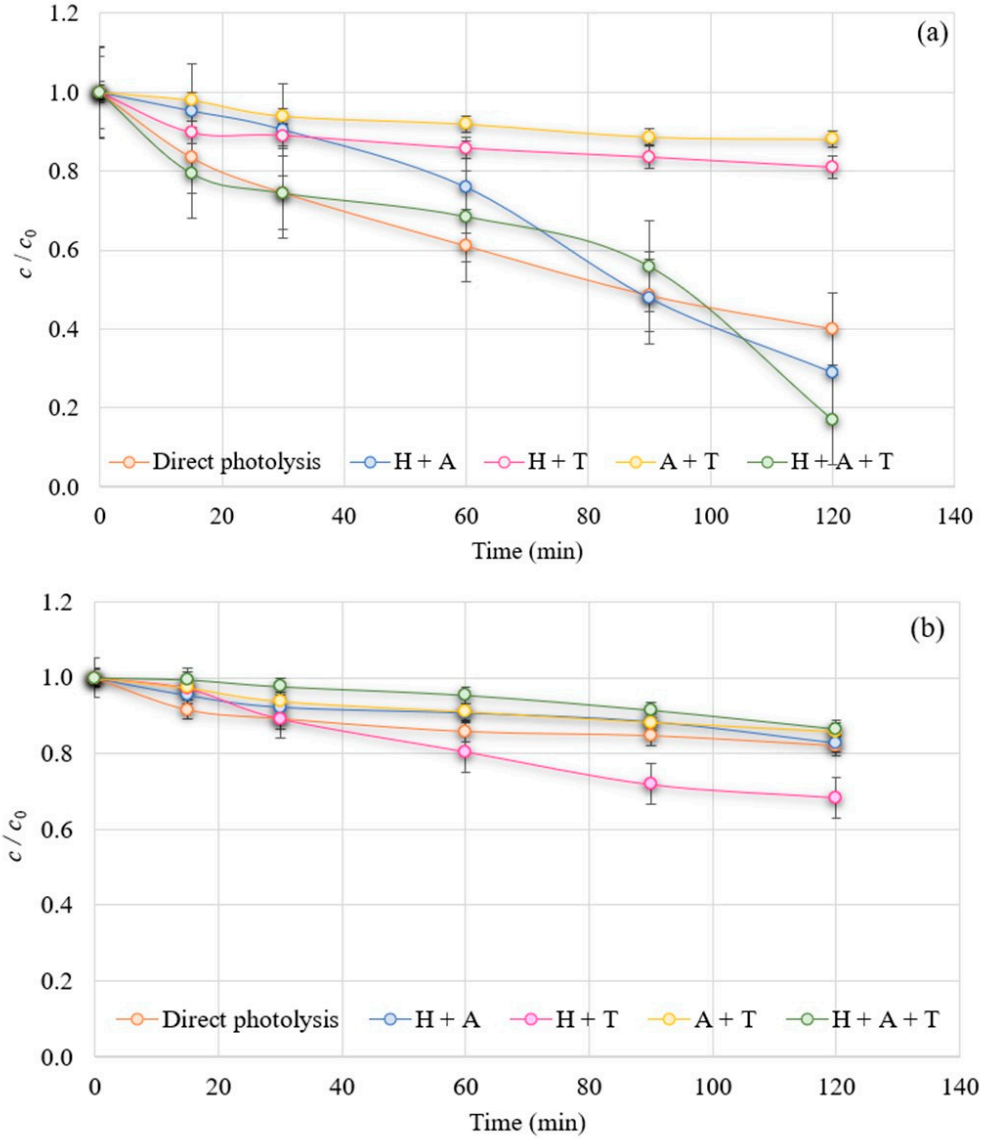


Figure 10. Influence of a mixture of Humiblack® (H), Agasi® (A), and Tifi® (T) on direct photolysis of (**a**) mancozeb and (**b**) metalaxyl in ultrapure water.

The addition of biostimulants to the mancozeb and metalaxyl mixture increased pH, so initial pH values ranged from 8.0 to 10.0 (Figure S8a). During degradation, pH values slightly decreased. The initial temperature was 25 °C, and it increased to 35 °C during the process (Figure S8b).

Further, the degradation rate of mancozeb and metalaxyl in the presence of a biostimulant mixture was examined in rainwater. Mancozeb showed high reactivity with the addition of all biostimulant combinations. Its degradation increased from 11% up to 35–56% (Figure 11a) depending on the biostimulant mixture. Metalaxyl was more stable, and changes in its stability did not appear with the addition of biostimulants, except in one case. Namely, with the addition of the Humiblack® + Tifi® combination, its degradation was 53% (Figure 11b). pH value was constant around 8.0 (Figure S9a). The temperature in the sun simulator was 25 °C, and it increased to 35 °C during the process (Figure S9b).

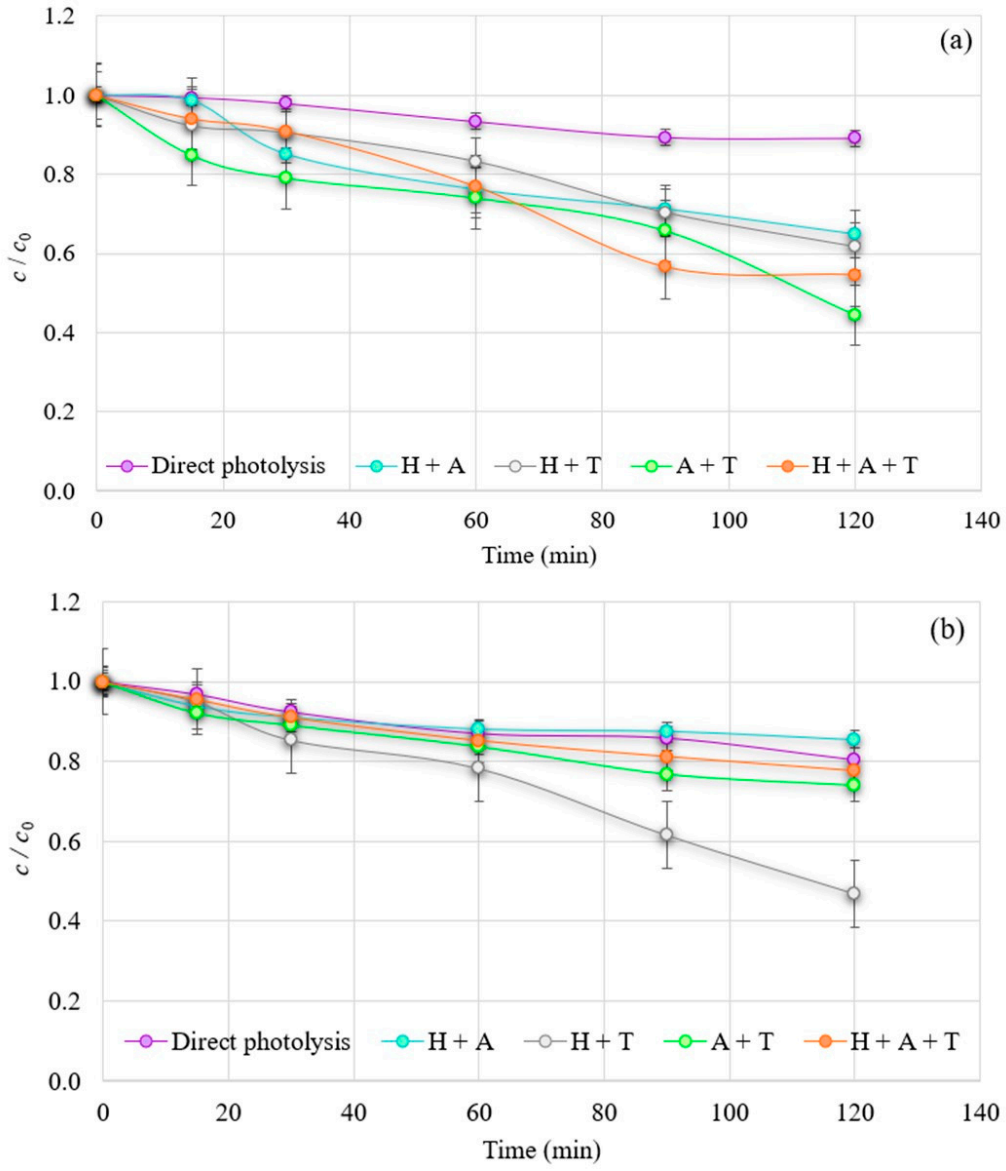


Figure 11. Influence of a mixture of Humiblack® (H), Agasi® (A), and Tifi® (T) mixture on direct photolysis of (**a**) mancozeb and (**b**) metalaxyl in rainwater.

These results suggest that the addition of the biostimulant mixture destabilized molecules of mancozeb and metalaxyl. Overall, the results indicate that the use of multiple biostimulants may not provide additional benefits compared to the use of a single biostimulant. In this work, we suggest the use of one biostimulant in combination with fungicides to increase onion quality and yield.

The present study has several limitations that should be mentioned. The stability experiments were performed under controlled laboratory and simulated conditions. The

obtained results gave valuable insights but may not fully capture the complexity of real environments. Also, a selected number of biostimulants and their combinations were investigated, which may limit the broader application of these study findings to other agricultural systems. Finally, the long-term environmental fate of fungicides and biostimulants and the potential impact of pesticide degradation products remains a key area for future research. Further research should also address the ecological impact of residual fungicides, particularly their effects on soil microbial activity and aquatic systems.

4. Conclusions

The combined application of biostimulants (HumiBlack®, Agasi®, and Tifi®) and fungicides (mancozeb and metalaxyl) significantly increased onion yield and growth, confirming the beneficial role of biostimulants in enhancing crop productivity under field conditions.

Mancozeb and metalaxyl showed high resistance to the hydrolysis process in both water types (ultrapure water and rainwater). Molecular dynamics simulations explicitly incorporating the aqueous environment suggest that mancozeb interacts more strongly with water than metalaxyl. Interaction energy analysis indicates a higher solute–solvent affinity for mancozeb, while RDFs reveal the presence of short-range, strong hydrogen-bond interactions between mancozeb and surrounding water molecules. These features are consistent with the observed higher hydrolytic susceptibility and support the experimentally observed faster degradation of mancozeb in aqueous systems. Metalaxyl exhibits weaker and more distant solvation interactions, in line with its greater environmental persistence. Considering these characteristics is essential for aligning pesticide use with the principles of sustainable agriculture.

Photolysis of mancozeb and metalaxyl was performed in the sun simulator mimicking environmental conditions. The photolysis rate was higher for mancozeb, while metalaxyl showed higher stability, which may be attributed to the presence of an aromatic ring in its structure. Quantum molecular descriptors derived from frontier molecular orbitals suggest that mancozeb possesses a smaller HOMO–LUMO gap and a higher electrophilicity index than metalaxyl, indicating a greater sensitivity for photoexcitation and charge-transfer processes. These intrinsic electronic features help explain the higher efficiency of direct photolysis of mancozeb in ultrapure water compared to the markedly higher photostability of metalaxyl. Visualization of the frontier molecular orbitals further refines this interpretation by revealing fundamental differences in orbital localization. In mancozeb, both HOMO and LUMO are broadly delocalized over the molecular framework, enabling extensive charge redistribution upon light absorption and increasing the likelihood of bond weakening and degradation. The frontier orbitals of metalaxyl are strongly localized on the aromatic ring, limiting photoinduced electronic processes to a small region of the molecule and thereby contributing to its resistance toward direct photolysis.

In rainwater, photolysis efficiency was reduced. Ions present in rainwater, such as chloride, sodium, and potassium ions, may inhibit the photolysis of mancozeb and metalaxyl. The addition of biostimulants alone had some effects on mancozeb, whereas metalaxyl stability was unaffected by the biostimulants. With the addition of a biostimulant mixture to the mancozeb and metalaxyl solution, their behavior was different, depending on the biostimulant combinations. Some biostimulant mixtures lead to the destabilization and degradation of mancozeb and metalaxyl molecules. These results suggest that a fungicide mixture could be used in combination with one biostimulant on the field, potentially contributing to an economically and environmentally sustainable process in onion production. These results underscore the importance of applying fungicide formulations in combination with biostimulants in agriculture as a promising approach in sustainable agriculture and economic food production.

Supplementary Materials: The following supporting information can be downloaded at https://www.mdpi.com/article/10.3390/su18094591/s1, Figure S1: Calibration curve for the determination of iron; Figure S2: Calibration curve for the determination of sodium; Figure S3: Calibration curve for the determination of potassium; Figure S4: Calibration curve for the determination of the conductivity of a standard KCl solution at different temperatures; Table S1: The physicochemical characteristics of the analyzed ultrapure water and rainwater; Figure S5: The structural formula of mancozeb (a) and metalaxyl (b); Figure S6: Change in the (a) pH and (b) T (°C) during direct photolysis of mancozeb and metalaxyl in ultrapure water under the influence of Humiblack®, Agasi®, and Tifi®; Figure S7: Change in the (a) pH and (b) T (°C) during direct photolysis of mancozeb and metalaxyl in rainwater under the influence of Humiblack®, Agasi®, and Tifi®; Figure S8: Change in the (a) pH and (b) T (°C) during direct photolysis of mancozeb and metalaxyl in ultrapure water under the influence of Humiblack® (H), Agasi® (A), and Tifi® (T) mixture; Figure S9: Change in the (a) pH and (b) T (°C) during direct photolysis of mancozeb and metalaxyl in rainwater under the influence of Humiblack® (H), Agasi® (A), and Tifi® (T) mixture.

Author Contributions: Conceptualization, M.M.S., Đ.V., Ž.M.I., S.A. and S.J.A.; Methodology, M.M.S., Đ.V., Ž.M.I., S.A. and S.J.A.; Software, S.A. and S.J.A.; Validation, M.M.S., Đ.V., A.B., T.G., S.A. and S.J.A.; Formal analysis, M.M.S., Đ.V., A.B., I.S., T.G., S.A. and S.J.A.; Investigation, M.M.S., Đ.V., A.B., I.S., T.G., S.A. and S.J.A.; Resources, Đ.V., Ž.M.I., S.A. and S.J.A.; Data curation, M.M.S., Đ.V., A.B., S.A. and S.J.A.; Writing—original draft, M.M.S., Đ.V., A.B., Ž.M.I., I.S., T.G., S.A. and S.J.A.; Writing—review & editing, M.M.S., Đ.V., S.A. and S.J.A.; Visualization, M.M.S., Đ.V., A.B., S.A. and S.J.A.; Supervision, Ž.M.I., I.S., S.A. and S.J.A.; Project administration, S.A. and S.J.A.; Funding acquisition, S.A. and S.J.A. All authors have read and agreed to the published version of the manuscript.

Funding: The authors gratefully acknowledge the financial support of the Ministry of Science, Technological Development and Innovation of the Republic of Serbia (Grants No. 451-03-33/2026-03/200125 & 451-03-34/2026-03/200125 and Contract No. 451-03-34/2026-03/200117 dated 5 February 2026).

Data Availability Statement: The original contributions presented in the study are included in the article; further inquiries can be directed to the corresponding author.

Conflicts of Interest: The authors declare no conflicts of interest.

References

1. Vojnović, Đ.; Maksimović, I.; Tepić Horecki, A.; Karadžić Banjac, M.; Kovačević, S.; Daničić, T.; Podunavac-Kuzmanović, S.; Ilin, Ž. Onion (*Allium cepa* L.) Yield and Quality Depending on Biostimulants and Nitrogen Fertilization—A Chemometric Perspective. *Processes* **2023**, *11*, 684. [CrossRef]
2. Ortega-García, J.G.; Montes-Belmont, R.; Rodríguez-Monroy, M.; Ramírez-Trujillo, J.A.; Suárez-Rodríguez, R.; Sepúlveda-Jiménez, G. Effect of *Trichoderma* Asperellum Applications and Mineral Fertilization on Growth Promotion and the Content of Phenolic Compounds and Flavonoids in Onions. *Sci. Hortic.* **2015**, *195*, 8–16. [CrossRef]
3. Sagar, N.A.; Pareek, S.; Benkeblia, N.; Xiao, J. Onion (*Allium cepa*) Bioactives: Chemistry, Pharmacotherapeutic Functions, and Industrial Applications. *Food Front.* **2022**, *3*, 380–412. [CrossRef]
4. Vojnović, Đ.; Maksimović, I.; Tepić Horecki, A.; Žunić, D.; Adamović, B.; Milić, A.; Šumić, Z.; Sabadoš, V.; Ilin, Ž. Biostimulants Affect Differently Biomass and Antioxidant Status of Onion (*Allium cepa*) Depending on Production Method. *Horticulturae* **2023**, *9*, 1345. [CrossRef]
5. Bulgari, R.; Franzoni, G.; Ferrante, A. Biostimulants Application in Horticultural Crops under Abiotic Stress Conditions. *Agronomy* **2019**, *9*, 306. [CrossRef]
6. Kocira, S.; Szparaga, A.; Hara, P.; Treder, K.; Findura, P.; Bartoš, P.; Filip, M. Biochemical and Economical Effect of Application Biostimulants Containing Seaweed Extracts and Amino Acids as an Element of Agroecological Management of Bean Cultivation. *Sci. Rep.* **2020**, *10*, 17759. [CrossRef]
7. Gemin, L.G.; Mógor, Á.F.; De Oliveira Amatussi, J.; Mógor, G. Microalgae Associated to Humic Acid as a Novel Biostimulant Improving Onion Growth and Yield. *Sci. Hortic.* **2019**, *256*, 108560. [CrossRef]
8. Novello, G.; Cesaro, P.; Bona, E.; Massa, N.; Gosetti, F.; Scarafoni, A.; Todeschini, V.; Berta, G.; Lingua, G.; Gamalero, E. The Effects of Plant Growth-Promoting Bacteria with Biostimulant Features on the Growth of a Local Onion Cultivar and a Commercial Zucchini Variety. *Agronomy* **2021**, *11*, 888. [CrossRef]
9. Rouphael, Y.; Colla, G. Biostimulants in Agriculture. *Front. Plant Sci.* **2020**, *11*, 40. [CrossRef] [PubMed]

10. Abou Chehade, L.; Al Chami, Z.; De Pascali, S.A.; Cavoski, I.; Fanizzi, F.P. Biostimulants from Food Processing By-products: Agronomic, Quality and Metabolic Impacts on Organic Tomato (*Solanum lycopersicum* L.). *J. Sci. Food Agric.* **2018**, *98*, 1426–1436. [CrossRef]
11. Abd El-Baset, M.; Kasem, M. Improving Growth Characteristics and Vase Life of Dendranthema Grandiflorum "flyer" Using Humic and Fulvic Acids as Biostimulants Substances. *Sci. J. Flowers Ornam. Plants* **2022**, *9*, 87–102. [CrossRef]
12. Canellas, L.P.; Olivares, F.L.; Aguiar, N.O.; Jones, D.L.; Nebbioso, A.; Mazzei, P.; Piccolo, A. Humic and Fulvic Acids as Biostimulants in Horticulture. *Sci. Hortic.* **2015**, *196*, 15–27. [CrossRef]
13. López-Bucio, J.; Pelagio-Flores, R.; Herrera-Estrella, A. Trichoderma as Biostimulant: Exploiting the Multilevel Properties of a Plant Beneficial Fungus. *Sci. Hortic.* **2015**, *196*, 109–123. [CrossRef]
14. Katsenios, N.; Sparangis, P.; Vitsa, S.; Leonidakis, D.; Efthimiadou, A. Application of Biostimulants and Herbicides as a Promising Co-Implementation: The Incorporation of a New Cultivation Practice. *Agronomy* **2023**, *13*, 2634. [CrossRef]
15. Dugan, S.T.; Muhammetoglu, A.; Uslu, A. A Combined Approach for the Estimation of Groundwater Leaching Potential and Environmental Impacts of Pesticides for Agricultural Lands. *Sci. Total Environ.* **2023**, *901*, 165892. [CrossRef]
16. Pimentão, A.R.; Cuco, A.P.; Pascoal, C.; Cássio, F.; Castro, B.B. Current Trends and Mismatches on Fungicide Use and Assessment of the Ecological Effects in Freshwater Ecosystems. *Environ. Pollut.* **2024**, *347*, 123678. [CrossRef] [PubMed]
17. Syafrudin, M.; Kristanti, R.A.; Yuniarto, A.; Hadibarata, T.; Rhee, J.; Al-Onazi, W.A.; Algarni, T.S.; Almarri, A.H.; Al-Mohaimeed, A.M. Pesticides in Drinking Water—A Review. *Int. J. Environ. Res. Public Health* **2021**, *18*, 468. [CrossRef]
18. Arfanis, M.K.; Theodorakopoulos, G.V.; Anagnostopoulos, C.; Georgaki, I.; Karanasios, E.; Romanos, G.E.; Markellou, E.; Falaras, P. Photocatalytic Removal of Thiamethoxam and Flonicamid Pesticides Present in Agro-Industrial Water Effluents. *Catalysts* **2023**, *13*, 516. [CrossRef]
19. Jazić, J.M.; Đurkić, T.; Bašić, B.; Watson, M.; Apostolović, T.; Tubić, A.; Agbaba, J. Degradation of a Chloroacetanilide Herbicide in Natural Waters Using UV Activated Hydrogen Peroxide, Persulfate and Peroxymonosulfate Processes. *Environ. Sci. Water Res. Technol.* **2020**, *6*, 2800–2815. [CrossRef]
20. Zahedi, S.M.; Karimi, M.; Teixeira da Silva, J.A. The Use of Nanotechnology to Increase Quality and Yield of Fruit Crops. *J. Sci. Food Agric.* **2020**, *100*, 25–31. [CrossRef]
21. Hordyjewicz-Baran, Z.; Wasilewski, T.; Zarębska, M.; Seweryn, A.; Zajszły-Turko, E.; Stanek-Wandzel, N.; Chrobak, J. Application of Aggregation Behavior of Nonionic Surfactants to Develop a Smart Detergent for Washing Fruits with Emphasis on Pesticide Residues Removal. *J. Surfactants Deterg.* **2024**, *27*, 57–69. [CrossRef]
22. Samari, M.; Heydari, R.; Gholami, F. Nanofiltration Membrane Functionalized with CuxP Nanoparticles: A Promising Approach for Enhanced Pesticide Removal and Long-Term Stability. *J. Clean. Prod.* **2024**, *445*, 141352. [CrossRef]
23. Tiryaki, O.; Temur, C. The Fate of Pesticide in the Environment. *J. Biol. Environ. Sci.* **2010**, *4*, 29–38.
24. Fenner, K.; Canonica, S.; Wackett, L.P.; Elsner, M. Evaluating Pesticide Degradation in the Environment: Blind Spots and Emerging Opportunities. *Science* **2013**, *341*, 752–758. [CrossRef]
25. Kaur, R.; Singh, D.; Kumari, A.; Sharma, G.; Rajput, S.; Arora, S.; Kaur, R. Pesticide Residues Degradation Strategies in Soil and Water: A Review. *Int. J. Environ. Sci. Technol.* **2023**, *20*, 3537–3560. [CrossRef]
26. Gikas, G.D.; Parlakidis, P.; Mavropoulos, T.; Vryzas, Z. Particularities of Fungicides and Factors Affecting Their Fate and Removal Efficacy: A Review. *Sustainability* **2022**, *14*, 4056. [CrossRef]
27. Gavrilescu, M. Fate of Pesticides in the Environment and Its Bioremediation. *Eng. Life Sci.* **2005**, *5*, 497–526. [CrossRef]
28. Žunić, D.; Sabadoš, V.; Vojnović, Đ.; Maksimović, I.; Ilin, D.; Tepić Horecki, A.; Ilin, Ž. Potato (*Solanum tuberosum* L.) Cultivar Yield and Quality Affected by Irrigation and Fertilization—From Field to Chip Bag. *Horticulturae* **2023**, *9*, 1153. [CrossRef]
29. Vojnović, Đ.; Maksimović, I.; Tepić Horecki, A.; Milić, A.; Šumić, Z.; Žunić, D.; Adamović, B.; Ilin, Ž. Biostimulants Improve Bulb Yield, Concomitantly Affecting the Total Phenolics, Flavonoids, and Antioxidant Capacity of Onion (*Allium cepa*). *Horticulturae* **2024**, *10*, 391. [CrossRef]
30. Sumithra, M.; Sundaraganesan, N.; Rajesh, R.; Vetrivelan, V.; Ilangovan, V.; Javed, S.; Muthu, S. Electron Acceptor, Excitation Energies, Oscillatory Strength, Spectroscopic and Solvent Effects on 5-Amino-4,6-Dichloro-2-(Propylthio) Pyrimidine—Anticancer Agent. *Chem. Phys. Impact* **2023**, *6*, 100145. [CrossRef]
31. Bannwarth, C.; Caldeweyher, E.; Ehlert, S.; Hansen, A.; Pracht, P.; Seibert, J.; Spicher, S.; Grimme, S. Extended Tight-Binding Quantum Chemistry Methods. *WIREs Comput. Mol. Sci.* **2021**, *11*, e1493. [CrossRef]
32. Bannwarth, C.; Ehlert, S.; Grimme, S. GFN2-xTB—An Accurate and Broadly Parametrized Self-Consistent Tight-Binding Quantum Chemical Method with Multipole Electrostatics and Density-Dependent Dispersion Contributions. *J. Chem. Theory Comput.* **2019**, *15*, 1652–1671. [CrossRef]
33. Ehlert, S.; Stahn, M.; Spicher, S.; Grimme, S. Robust and Efficient Implicit Solvation Model for Fast Semiempirical Methods. *J. Chem. Theory Comput.* **2021**, *17*, 4250–4261. [CrossRef]

34. Grimme, S.; Bannwarth, C.; Shushkov, P. A Robust and Accurate Tight-Binding Quantum Chemical Method for Structures, Vibrational Frequencies, and Noncovalent Interactions of Large Molecular Systems Parametrized for All Spd-Block Elements (Z = 1–86). *J. Chem. Theory Comput.* **2017**, *13*, 1989–2009. [CrossRef] [PubMed]
35. Armaković, S.; Armaković, S.J. Atomistica.Online—Web Application for Generating Input Files for ORCA Molecular Modelling Package Made with the Anvil Platform. *Mol. Simul.* **2023**, *49*, 117–123. [CrossRef]
36. Armaković, S.; Armaković, S.J. Online and Desktop Graphical User Interfaces for Xtb Programme from Atomistica.Online Platform. *Mol. Simul.* **2024**, *50*, 560–570. [CrossRef]
37. Armaković, S.; Armaković, S.J. Predicting Properties of Imidazolium-Based Ionic Liquids via Atomistica Online: Machine Learning Models and Web Tools. *Computation* **2025**, *13*, 216. [CrossRef]
38. Armaković, S.; Armaković, S. Recent Developments in Atomistic Modeling: Machine Learning Models and Datasets, Methods, Software Releases, and Scientific Events. *Aidasco Rev.* **2025**, *3*, 21–35. [CrossRef]
39. de Souza, B. GOAT: A Global Optimization Algorithm for Molecules and Atomic Clusters. *Angew. Chem. Int. Ed.* **2025**, *64*, e202500393. [CrossRef]
40. Goedecker, S. Minima Hopping: An Efficient Search Method for the Global Minimum of the Potential Energy Surface of Complex Molecular Systems. *J. Chem. Phys.* **2004**, *120*, 9911–9917. [CrossRef]
41. Wales, D.J.; Doye, J.P.K. Global Optimization by Basin-Hopping and the Lowest Energy Structures of Lennard-Jones Clusters Containing up to 110 Atoms. *J. Phys. Chem. A* **1997**, *101*, 5111–5116. [CrossRef]
42. Neese, F. The SHARK Integral Generation and Digestion System. *J. Comput. Chem.* **2022**, *44*, 381–396. [CrossRef]
43. Teale, A.M.; Helgaker, T.; Savin, A.; Adamo, C.; Aradi, B.; Arbuznikov, A.V.; Ayers, P.W.; Baerends, E.J.; Barone, V.; Calaminici, P.; et al. DFT Exchange: Sharing Perspectives on the Workhorse of Quantum Chemistry and Materials Science. *Phys. Chem. Chem. Phys.* **2022**, *24*, 28700–28781. [CrossRef]
44. Neese, F. Software Update: The ORCA Program System—Version 5.0. *WIREs Comput. Mol. Sci.* **2022**, *12*, e1606. [CrossRef]
45. Neese, F. Software Update: The ORCA Program System, Version 4.0. *WIREs Comput. Mol. Sci.* **2018**, *8*, e1327. [CrossRef]
46. Neese, F. The ORCA Program System. *WIREs Comput. Mol. Sci.* **2012**, *2*, 73–78. [CrossRef]
47. Neese, F.; Wennmohs, F.; Becker, U.; Riplinger, C. The ORCA Quantum Chemistry Program Package. *J. Chem. Phys.* **2020**, *152*, 224108. [CrossRef]
48. Grimme, S.; Hansen, A.; Ehlert, S.; Mewes, J.-M. r2SCAN-3c: A "Swiss Army Knife" Composite Electronic-Structure Method. *J. Chem. Phys.* **2021**, *154*, 064103. [CrossRef] [PubMed]
49. Mardirossian, N.; Head-Gordon, M. ωB97X-V: A 10-Parameter, Range-Separated Hybrid, Generalized Gradient Approximation Density Functional with Nonlocal Correlation, Designed by a Survival-of-the-Fittest Strategy. *Phys. Chem. Chem. Phys.* **2014**, *16*, 9904–9924. [CrossRef]
50. Weigend, F.; Ahlrichs, R. Balanced Basis Sets of Split Valence, Triple Zeta Valence and Quadruple Zeta Valence Quality for H to Rn: Design and Assessment of Accuracy. *Phys. Chem. Chem. Phys.* **2005**, *7*, 3297–3305. [CrossRef] [PubMed]
51. Weigend, F. Accurate Coulomb-Fitting Basis Sets for H to Rn. *Phys. Chem. Chem. Phys.* **2006**, *8*, 1057–1065. [CrossRef]
52. Humphrey, W.; Dalke, A.; Schulten, K. VMD—Visual Molecular Dynamics. *J. Mol. Graph.* **1996**, *14*, 33–38. [CrossRef]
53. Eargle, J.; Wright, D.; Luthey-Schulten, Z. Multiple Alignment of Protein Structures and Sequences for VMD. *Bioinformatics* **2006**, *22*, 504–506. [CrossRef]
54. Varshney, A.; Brooks, F.P.; Wright, W.V. Linearly Scalable Computation of Smooth Molecular Surfaces. *IEEE Comput. Graph. Appl.* **1994**, *14*, 19–25. [CrossRef]
55. Levine, B.G.; Stone, J.E.; Kohlmeyer, A. Fast Analysis of Molecular Dynamics Trajectories with Graphics Processing Units—Radial Distribution Function Histogramming. *J. Comput. Phys.* **2011**, *230*, 3556–3569. [CrossRef]
56. Frishman, D.; Argos, P. Knowledge-Based Secondary Structure Assignment. *Proteins Struct. Funct. Genet.* **1995**, *23*, 566–579. [CrossRef] [PubMed]
57. Lu, T. A Comprehensive Electron Wavefunction Analysis Toolbox for Chemists, Multiwfn. *J. Chem. Phys.* **2024**, *161*, 082503. [CrossRef] [PubMed]
58. Lu, T.; Chen, Q. Van Der Waals Potential: An Important Complement to Molecular Electrostatic Potential in Studying Intermolecular Interactions. *J. Mol. Model.* **2020**, *26*, 315. [CrossRef]
59. Lu, T.; Manzetti, S. Wavefunction and Reactivity Study of Benzo[a]Pyrene Diol Epoxide and Its Enantiomeric Forms. *Struct. Chem.* **2014**, *25*, 1521–1533. [CrossRef]
60. Lu, T.; Chen, F. Multiwfn: A Multifunctional Wavefunction Analyzer. *J. Comput. Chem.* **2012**, *33*, 580–592. [CrossRef]
61. *Schrödinger Release 2022-1: Maestro*; Schrödinger, LLC: New York, NY, USA, 2022.
62. Harder, E.; Damm, W.; Maple, J.; Wu, C.; Reboul, M.; Xiang, J.Y.; Wang, L.; Lupyan, D.; Dahlgren, M.K.; Knight, J.L.; et al. OPLS3: A Force Field Providing Broad Coverage of Drug-like Small Molecules and Proteins. *J. Chem. Theory Comput.* **2016**, *12*, 281–296. [CrossRef]

63. Roos, K.; Wu, C.; Damm, W.; Reboul, M.; Stevenson, J.M.; Lu, C.; Dahlgren, M.K.; Mondal, S.; Chen, W.; Wang, L.; et al. OPLS3e: Extending Force Field Coverage for Drug-Like Small Molecules. *J. Chem. Theory Comput.* **2019**, *15*, 1863–1874. [CrossRef]
64. Jorgensen, W.L.; Tirado-Rives, J. The OPLS [Optimized Potentials for Liquid Simulations] Potential Functions for Proteins, Energy Minimizations for Crystals of Cyclic Peptides and Crambin. *J. Am. Chem. Soc.* **1988**, *110*, 1657–1666. [CrossRef]
65. Jorgensen, W.L.; Maxwell, D.S.; Tirado-Rives, J. Development and Testing of the OPLS All-Atom Force Field on Conformational Energetics and Properties of Organic Liquids. *J. Am. Chem. Soc.* **1996**, *118*, 11225–11236. [CrossRef]
66. Bowers, K.J.; Chow, E.; Xu, H.; Dror, R.O.; Eastwood, M.P.; Gregersen, B.A.; Klepeis, J.L.; Kolossvary, I.; Moraes, M.A.; Sacerdoti, F.D.; et al. Scalable Algorithms for Molecular Dynamics Simulations on Commodity Clusters. In *Proceedings of the 2006 ACM/IEEE Conference on Supercomputing; Association for Computing Machinery: Tampa, FL, USA, 11–17 November 2006*; IEEE: New York, NY, USA, 2006; p. 43.
67. Perić, M.; Savanović, M.M.; Bilić, A.; Armaković, S.J.; Armaković, S. Comparative Analysis and Validation of Analytical Techniques for Quantification Active Component in Pharmaceuticals: Green Approach. *J. Indian Chem. Soc.* **2024**, *101*, 101173. [CrossRef]
68. Harman, G.E.; Howell, C.R.; Viterbo, A.; Chet, I.; Lorito, M. Trichoderma Species—Opportunistic, Avirulent Plant Symbionts. *Nat. Rev. Microbiol.* **2004**, *2*, 43–56. [CrossRef]
69. Fiorentino, N.; Ventorino, V.; Woo, S.L.; Pepe, O.; De Rosa, A.; Gioia, L.; Romano, I.; Lombardi, N.; Napolitano, M.; Colla, G.; et al. Trichoderma-Based Biostimulants Modulate Rhizosphere Microbial Populations and Improve N Uptake Efficiency, Yield, and Nutritional Quality of Leafy Vegetables. *Front. Plant Sci.* **2018**, *9*, 743. [CrossRef] [PubMed]
70. Hafez, E.; Geries, L. Effect of Nitrogen Fertilization and Biostimulative Compounds on Onion Productivity. *Cercet. Agron. Mold.* **2018**, *51*, 75–90. [CrossRef]
71. Zandonadi, D.B.; Canellas, L.P.; Façanha, A.R. Indolacetic and Humic Acids Induce Lateral Root Development through a Concerted Plasmalemma and Tonoplast H+ Pumps Activation. *Planta* **2007**, *225*, 1583–1595. [CrossRef] [PubMed]
72. López-Fernández, O.; Yáñez, R.; Rial-Otero, R.; Simal-Gándara, J. Kinetic Modelling of Mancozeb Hydrolysis and Photolysis to Ethylenethiourea and Other By-Products in Water. *Water Res.* **2016**, *102*, 561–571. [CrossRef]
73. Sukul, P.; Spiteller, M. Metalaxyl: Persistence, Degradation, Metabolism, and Analytical Methods. *Rev. Environ. Contam. Toxicol.* **2000**, *164*, 1–26.
74. Romain, S.J.S.; Basirico, L.M.; Kim, Y.-H.; Armbrust, K.L. Impacts of Salinity on the Hydrolysis of Chlorpyrifos. *ACS Agric. Sci. Technol.* **2023**, *3*, 165–170. [CrossRef]
75. Bin Khalid, Z.; Kelso, C.; Van De Merwe, J.; Hai, F.I. Impact of Ions Co-Occurring in Water on Antibiotics Degradation by UV-Based Advanced Oxidation Process. *Chemosphere* **2026**, *394*, 144798. [CrossRef] [PubMed]
76. Campbell, T.D.; Hart, C.A.; Febrian, R.; Cheneler, M.L.; Bracher, P.J. The Opposite Effect of K+ and Na+ on the Hydrolysis of Linear and Cyclic Dipeptides. *Tetrahedron Lett.* **2018**, *59*, 2264–2267. [CrossRef]
77. Islam, J.B.; Furukawa, M.; Tateishi, I.; Katsumata, H.; Kaneco, S. Photocatalytic Degradation of a Typical Agricultural Chemical: Metalaxyl in Water Using TiO_2 under Solar Irradiation. *SN Appl. Sci.* **2020**, *2*, 925. [CrossRef]
78. Conradie, T.A.; Lawson, K.; Allsopp, M.; Jacobs, K. Exploring the Impact of Fungicide Exposure and Nutritional Stress on the Microbiota and Immune Response of the Cape Honey Bee (Apis Mellifera Capensis). *Microbiol. Res.* **2024**, *280*, 127587. [CrossRef]
79. Zhao, C.; Wang, Z.; Wang, C.; Li, X.; Wang, C.-C. Photocatalytic Degradation of DOM in Urban Stormwater Runoff with TiO_2 Nanoparticles under UV Light Irradiation: EEM-PARAFAC Analysis and Influence of Co-Existing Inorganic Ions. *Environ. Pollut.* **2018**, *243*, 177–188. [CrossRef]
80. Uzelac, M.M.; Srđenović Čonić, B.; Kladar, N.; Armaković, S.; Armaković, S.J. Removal of Hydrochlorothiazide from Drinking and Environmental Water: Hydrolysis, Direct and Indirect Photolysis. *Energy Environ.* **2022**, *34*, 0958305X2210840. [CrossRef]
81. Peng, N.; Wang, K.; Lin, S.; Wu, L. Effects of Inorganic Ions on the Photolysis of Propranolol in FA Solution. *Env. Sci. Pollut. Res.* **2018**, *25*, 26069–26078. [CrossRef] [PubMed]

Disclaimer/Publisher's Note: The statements, opinions and data contained in all publications are solely those of the individual author(s) and contributor(s) and not of MDPI and/or the editor(s). MDPI and/or the editor(s) disclaim responsibility for any injury to people or property resulting from any ideas, methods, instructions or products referred to in the content.